Signaling Domain of the Aspartate Receptor Is a Helical Hairpin with a Localized Kinase Docking Surface: Cysteine and Disulfide Scanning Studies†

Randal B. Bass, Matthew D. Coleman, and Joseph J. Falke*

Department of Chemistry and Biochemistry, University of Colorado at Boulder, Boulder, Colorado 80309-0215

Received April 8, 1999; Revised Manuscript Received May 26, 1999

ABSTRACT: Cysteine and disulfide scanning has been employed to probe the signaling domain, a highly conserved motif found in the cytoplasmic region of the aspartate receptor of bacterial chemotaxis and related members of the taxis receptor family. Previous work has characterized the N-terminal section of the signaling domain [Bass, R. B., and Falke, J. J. (1998) *J. Biol. Chem. 273*, 25006−25014], while the present study focuses on the C-terminal section and the interactions between these two regions. Engineered cysteine residues are incorporated at positions Gly388 through Ile419 in the signaling domain, thereby generating a library of receptors each containing a single cysteine per receptor subunit. The solvent exposure of each cysteine is ascertained by chemical reactivity measurements, revealing a periodic pattern of buried hydrophobic and exposed polar residues characteristic of an amphipathic α-helix, denoted helix α8. The helix begins between positions R392 and Val401, then continues through the last residue scanned, Ile419. Activity assays carried out both in vivo and in vitro indicate that both the buried and exposed faces of this amphipathic helix are critical for proper receptor function and the buried surface is especially important for kinase downregulation. Patterns of disulfide bond formation suggest that helix α8, together with the immediately N-terminal helix α7, forms a helical hairpin that associates with a symmetric hairpin from the other subunit of the homodimer, generating an antiparallel four helix bundle containing helices α7, α7′, α8, and α8′. Finally, the protein-interactions-by-cysteine-modification (PICM) method suggests that the loop between helices α7 and α8 interacts with the kinase CheA and/or the coupling protein CheW, expanding the receptor surface implicated in kinase docking.

The transmembrane aspartate receptor of *Escherichia coli* and *Salmonella typhimurium* chemotaxis is a member of the large receptor superfamily that modulates two-component signaling systems in prokaryotes and eukaryotes (*1*−*9*). A subfamily of these receptors, the methyl-accepting taxis receptors, share the highest sequence homology with the aspartate receptor and function in chemo-, thermo-, osmo-, photo-, and pH-taxis in a wide range of prokaryotic organisms (*5, 6, 10, 11*). The aspartate receptor is the best characterized member of this subfamily and has become a paradigm for two-component pathway receptors in general.

The aspartate receptor exists as a stable homodimer in which each subunit is approximately 60 kDa as schematically illustrated in Figure 1. The receptor possesses a periplasmic ligand binding domain, a transmembrane region, and a cytoplasmic domain that possesses adaptation sites and a kinase docking surface. The transmembrane and adaptation signals relayed by the cytoplasmic domain serve to control the histidine kinase CheA, which associates with the receptor in a complex stabilized by the coupling protein CheW (*12*−*16*). When the receptor-CheA-CheW ternary complex is active, it phosphorylates the response regulator CheY which diffuses to the flagellar motor where it docks and regulates cellular swimming (*3, 6, 7*). More generally, a conserved mechanism of transmembrane kinase regulation is shared by the aspartate receptor and other receptors that regulate histidine kinases in two-component signaling pathways, since functional dimeric receptors have been constructed by swapping the cytoplasmic domains of different superfamily members (*17*−*20*). Moreover, a chimera in which the cytoplasmic domain of the aspartate receptor is replaced with the cytoplasmic domain of the human insulin receptor exhibits aspartate-mediated tyrosine kinase activity, suggesting that similar transmembrane signals may be employed by receptors from unrelated classes (*21*).

The structures and mechanisms of the transmembrane signaling domain, consisting of the periplasmic ligand binding domain and the membrane-spanning helices, are well characterized for the aspartate receptor and for the closely related serine and ribose/galactose chemotaxis receptors (*22*−*29*). The architecture of the periplasmic and transmembrane regions consists of α-helical bundles oriented roughly perpendicular to the bilayer (*22*−*24, 30*). Transmembrane signaling begins in the periplasmic domain, where the binding of a single aspartate molecule generates an asymmetric piston displacement, and perhaps a small tilt, of the second transmembrane helix (α4/TM2) toward the cytoplasm (*31*). Evidence that the piston displacement serves to transmit the transmembrane signal is provided by lock-on and lock-off disulfides that trap the extremes of the piston displacement and thereby lock the kinase on or off (*22*). Further support comes from (i) ligand induced changes in disulfide formation rates between engineered cysteines on α4/TM2 and an adjacent helix and (ii) site-directed spin-labeling

† Support provided by NIH Grant GM R01-40731 (to J.J.F.).

* To whom correspondence should be addressed. Phone: (303) 492-3503. Fax: (303) 492-5894. E-mail: falke@colorado.edu.

10.1021/bi9908179 CCC: $18.00
Published on Web 07/01/1999

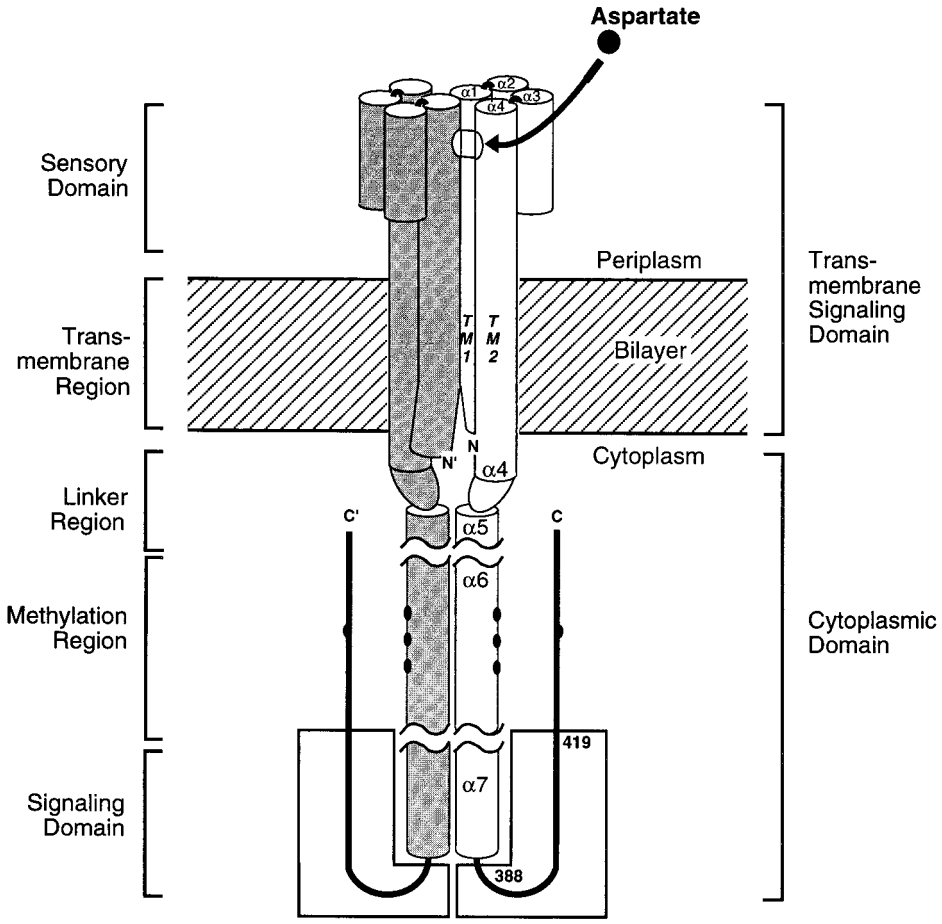

FIGURE 1: Schematic model of the aspartate receptor. Cylinders represent helices determined by previous crystallographic or cysteine and disulfide scanning studies (*22*, *23*, *30*). The two identical 60 kDa subunits of the dimer are depicted in white and gray, respectively. Filled ovals represent the sites of adaptive methylation on each subunit (*58*). The boxed regions highlight the positions included in the current cysteine and disulfide scanning study, G388C−I419C.

studies that detect ligand-induced distance changes between pairs of spin labels on α4/TM2 and adjacent helices (*32*, *33*). The aspartate receptor is also regulated by the maltose-binding protein (MBP), and a model of this interaction suggests that MBP docking generates a piston displacement of the second transmembrane helix similar to that observed for aspartate binding (*34*).

Although a high-resolution structure of the cytoplasmic domain is not yet available for any member of the receptor superfamily, there is a growing body of structural and mechanistic data on this domain of the aspartate receptor. Recent studies have shown that site-directed sulfhydryl chemistry and spectroscopy methods can elucidate structural and functional features of membrane proteins (*22*−*24*, *27*−*29*, *35*−*42*). In the cytoplasmic domain, cysteine- and disulfide-scanning studies have characterized the extension of the transmembrane-signaling helix α4/TM2 into the cytoplasm, followed by a structured linker region and at least three helical regions termed α5 through α7 (*43*−*45*). It is not yet clear whether these three helical regions represent three distinct helices separated by nonhelical linkers, or rather form a long, continuous helix. For simplicity, here they will be considered separate helices. Helices α5 and α6 lie at the subunit interface where they are tightly associated with the symmetric α5′ and α6′ helices from the other subunit of the dimer. Helix α6 senses and integrates the transmembrane, adaptation, pH, and temperature signals recognized by the receptor and is tightly coupled to kinase regulation (*46*−*48*). Helix α7 comprises the N-terminal half of the signaling domain, an independent structural motif within the cytoplasmic domain which has been isolated as a stable fragment and shown to bind CheA and CheW and to modulate the histidine kinase activity of CheA (*45*, *49*, *50*). Cysteine-scanning determined that both the buried and exposed faces of helix α7 are critical for kinase activation and regulation, although the engineered cysteines that lock the receptor in the kinase activating state are localized to the buried face. It follows that the buried face of helix α7 is especially important for receptor-mediated downregulation of kinase activity. Disulfide scanning determined that the C-terminal end of α7 and the ensuing loop are at or near the subunit interface. This C-terminal region of the helix was found to be essential for the docking or regulation of the kinase CheA, since attachment of bulky probes at exposed positions here block kinase activation (*45*).

The present study continues the cysteine- and disulfide-scanning analysis of the signaling domain by examining its C-terminal half located beyond the end of helix α7. The measured chemical reactivities of engineered cysteines display a periodic pattern of solvent exposure and burial, suggesting the presence of a second α-helix in this region, termed α8. Moreover, the exposed and buried surfaces of this helix possess numerous conserved polar and apolar positions, respectively, providing support for its assignment

as an amphipathic helix. Although both faces of this newly defined helix are important for receptor function, the buried face is especially critical for kinase downregulation since multiple cysteine substitutions here lock the receptor in its kinase-activating state. Together, helices α7 and α8 form a helical hairpin, as indicated by the observation that interhelix disulfide bonds form rapidly between specific pairs of engineered cysteines on their respective buried faces. Finally, the application of the protein-interactions-by-cysteine-modification (PICM)[1] assay to surface positions within the α7-α8 loop and on the α8 helix reveals another region critical for the docking or regulation of the kinase CheA (*45*).

MATERIALS AND METHODS

Materials. Strains of *E. coli* were kindly provided by Dr. John S. Parkinson, University of Utah (Salt Lake City, UT). Strains used for receptor expression and characterization were RP3808 [Δ(*cheA-cheZ*)*DE2209 tsr-1 leuB6 his-4 eda-50 rpsL136* [*thi-1* Δ(*gal-attl*)*DE99 ara-14 lacY1 mtl-1 xyl-5 tonA31 tsx-78*]/*mks*/) and RP8611 [Δ*tsrDE7028* Δ(*tar-tap*)-*DE5201 zbd::Tn5* Δ(*trg*)*DE100 leuB6 his-4 rpsL136* [*thi-1 ara-14 lacY1 mtl-1 xyl-5 tonA31 tsx-78*]/*CP362 of G. Hazelbauer via F. Dahlquist, pa*/) (*51*) The receptor expression plasmid pSCF6 has been previously described (*22*), as have the materials and protocols used to produce purified CheA, CheW, CheY, and CheR (*45*). The sulfhydryl-specific probes, 5-iodoacetamido fluorescein (5-IAF), and 5-fluorescein maleimide (5-FM) were obtained from Molecular Probes. Enzyme substrates *S*-adenosyl-L-[methyl-^{3}H]methionine and [γ-^{32}P]ATP were purchased from Amersham. Deoxy-oligonucleotides were synthesized by Life Technologies Inc. Kunkel mutagenesis reagents (T7 DNA Polymerase, T4 DNA ligase and deoxy-nucleotide triphosphates) were purchased from Bio-Rad. Unless specifically noted, all other reagents were obtained from Sigma and were of reagent grade.

Creation of Cysteine-Containing Receptors. Single cysteine-containing receptors were created by oligonucleotide-directed mutagenesis of the plasmid pSCF6 as described previously (*45*).

The double-cysteine-containing receptors N36C/F394C, A411C/I363C, A411C/I366C, A411C/A370C, A411C/T373C, A411C/A377C, and A411C/A380C were created by combining restriction fragments of the appropriate mutant derivative of pSCF6 (22). To generate the N36C/F394C mutant, a double digest employing *Pst*1 and *Mlu*1 (New England Biolabs) produced a 0.9 kb fragment containing the N36C mutation or a 4.1 kb fragment containing the F394C mutation. The digest containing the target 0.9 kb fragment was treated with calf intestinal phosphatase (CIP) to prevent self-ligation in subsequent steps. To generate the A411C/XXX mutants, a double digest employing *Pst*1 and *Msc*1 (New England Biolabs) produced a 3.5 kb fragment containing the A411C mutation or a 1.5 kb fragment containing the XXX site, and the latter fragment was treated with calf intestinal phosphatase (CIP). All fragments were resolved on a 1% TAE gel, stained with ethidium bromide, and illuminated with UV light, and the appropriate band was excised. The individual fragments were then isolated with the Gene Clean kit (Bio 101), mixed in the appropriate pairings and ligated overnight at 16 °C with T4 DNA ligase (New England Biolabs). Each resulting reconstructed pSCF6 derivative was transformed directly into the expression strain, RP3808, and receptor-containing membrane was prepared as described for the single cysteine-containing receptors. Under harsh oxidation conditions, a small percentage of the double cysteine containing receptor was observed on SDS−polyacrylamide gels to form trimers, tetramers, and higher order products, which could only occur if the engineered receptor possessed two cysteines per receptor subunit.

Purification of Engineered Receptors. Plasmids encoding cysteine substitutions were transformed into the *E. coli* strain RP3808, expressed and isolated in native membranes as previously described (*45*) except that the sonicator employed was a Mysonix model XL 2020. The resulting engineered receptor-containing membranes were snap frozen in liquid nitrogen and stored at −80 °C. The final storage buffer contained 20 mM sodium phosphate, pH 7.0, with NaOH, 10% v/v glycerol, 0.1 mM EDTA, and 0.5 mM PMSF.

Membrane samples were assayed for total protein using the BCA assay (Pierce) calibrated against bovine serum albumin standards (Pierce). After reaction development, absorbance measurements were made using a microplate reader (Molecular Devices). Protein purity was determined by quantitating the receptor and nonreceptor bands on a Coomassie-stained 10% Laemmli SDS−polyacrylamide gel (acrylamide-to-bisacrylamide ratio of 40:0.2) using a digital camera (Alpha Innotec).

Preparation of Cytoplasmic Chemotaxis Components. CheA, CheW, CheY, and CheR were overexpressed, produced in *E. coli*, and isolated as previously described (*22*, *43*).

Chemical Reactivity Assays. Reactivity assays were performed as previously described (*43*, *45*). Briefly, cysteine-containing receptors (5 μM receptor monomer) were incubated in reaction buffer (10 mM sodium phosphate, pH 6.5, with NaOH, 50 mM NaCl, 50 mM KCl, and 10 mM EDTA) containing the sulfhydryl-specific probe 5-IAF (300 μM final). The reaction was allowed to proceed for 5 min at 25 °C, at which time a 20 μL aliquot was removed and quenched with 1.25 μL of β-mercaptoethanol. The remaining 20 μL of the reaction was denatured with heat (95 °C) and SDS (0.6% w/v) and allowed to react for an additional 3 min before quenching. 5-IAF tagged receptors were resolved on 10% Laemmli acrylamide gels (acrylamide-to-bisacrylamide ratio of 40:0.2) and illuminated on a UV light box. Fluorescent bands were visualized and quantitated with a digital camera (Alpha Innotec). After fluorescent detection, gels were stained with Coomassie and receptor bands were quantitated with a digital camera to normalize for variations in receptor amounts. Chemical reactivity was defined as the ratio of receptor alkylation in the folded versus the unfolded states.

In Vivo Activity Assays. Chemotaxis swarm assays were performed in *E. coli* strain RP8611 as previously described (*51*, *52*). Controls using vector alone (pBluescript) or vector carrying the wild-type receptor (pSCF6) were performed to determine the swarm rates of receptorless cells and cells

[1] Abbreviations: PICM, protein-interactions-by-cysteine-modification; DTT, dithiothreitol; 5-IAF, 5-iodoacetamidofluorescein; 5-FM, fluorescein-5-maleimide; DMF, *N*,*N*-dimethyl-formamide; indel, insertion or deletion.

Table 1: Intrasubunit Disulfide Bond Formation under Mild Oxidation Conditions

receptor	fraction disulfide formation[a]
A411C/I363C	0.0 ± 0.1
A411C/I366C	0.0 ± 0.1
A411C/A370C	0.3 ± 0.1
A411C/T373C	0.2 ± 0.1
A411C/A377C	0.0 ± 0.1
A411C/A380C	0.0 ± 0.1

[a] Reaction for 1 min at 25 °C in a system containing 2 μM receptor monomer, 20 mM sodium phosphate, pH 7.0, with NaOH, 10% v/v glycerol, 5 mM EDTA, 1 mM Cu(II) (1,10 phenanthroline)$_3$, and ambient O_2.

possessing the native receptor, respectively. All swarm rates were determined on minimal media agar plates with or without 100 μM aspartate. Aspartate-specific swarm rates were determined by subtracting the (−) aspartate swarm rate from the (+) aspartate swarm rate to correct for pseudotaxis, and the resulting rate was then normalized to the wild-type rate for comparison (*22, 53*).

In Vitro Activity Assays. The in vitro receptor-coupled kinase assay was performed essentially as described with the following modifications (*15, 22, 45*). Membranes containing the reduced receptor were utilized except in experiments testing the effects of engineered disulfide bonds (see below). The receptor-coupled kinase reaction was initiated by the addition of [γ-^{32}P]ATP to a reaction mixture containing receptor, CheW, CheA, and CheY. After 10 s, an aliquot was removed and quenched with 2× Laemmli sample buffer supplemented with 25 mM EDTA to prevent further phosphorylation and dephosphorylation reactions (*54*). Stoichiometries were maintained such that receptor-regulated CheA autophosphorylation was the rate-determining step. [^{32}P]-Phospho-CheY, resulting from rapid phosphotransfer from phospho-CheA, was resolved on a 15% Laemmli SDS−polyacrylamide gel (acrylamide-to-bisacrylamide ratio of 40:1.25). Gels were dried and quantitated by phosphorimaging (Molecular Dynamics). A 10 μL wild-type reaction mixture contained 60 pmol of receptor monomer, 20 pmol of CheW, 100 pmol of CheY, 2.6 pmol of CheA, and 1000 pmol of ATP in reaction buffer (50 mM Tris, pH 7.5, with HCl, 50 mM KCL, and 5 mM $MgCl_2$).

Disulfide Formation in Single-Cysteine Receptors. For each single cysteine-containing receptor, a disulfide bond was formed between the symmetric cysteines in the two subunits of the dimer by exposing receptors to oxidizing conditions (Table 1). The resulting disulfide-linked dimers were used to test the effect of intersubunit disulfides on receptor-mediated kinase activation and regulation (*45*). Membrane samples containing 12 μM receptor monomer were incubated with 0.2 mM Cu(II) (1,10-phenanthroline)$_3$ and ambient O_2 (approximately 200 μM) for 20 min at 37 °C (*55, 56*). This oxidation was inactivated by the addition of 0.1 mM sodium persulfate, and the resulting membranes were used in the receptor-coupled kinase assay as above. The extent of disulfide formation was determined by analyzing an aliquot of the oxidized membranes on a 10% nonreducing Laemmli SDS−polyacrylamide gel (acrylamide-to-bisacrylamide ratio of 40:0.2) (*54*). Gels were subsequently Coomassie stained and monomer, dimer bands were quantitated with a digital camera (Alpha Innotec), and the percentage of dimer formation was calculated.

Disulfide Formation in Double-Cysteine Receptors. To quantitate disulfide formation triggered by oxidation of double cysteine-containing receptors, each receptor in *E. coli* membrane was diluted in a metal buffering solution containing buffer and EDTA to slow the reaction to measurable rates (2 μM receptor monomer, 20 mM sodium phosphate, pH 7.0, with NaOH, 10% v/v glycerol, and 5 mM EDTA) (*45, 57*). Oxidation was initiated by the addition of Cu(II) (1,10 phenanthroline)$_3$ to a concentration of 1 mM. This mild oxidation reaction was allowed to proceed at 25 °C for 1 min. Reactions were then quenched with 2× Laemmli sample buffer supplemented with 2 mM $NaAs0_4$ and 10 mM *N*-ethylmaleimide (*54, 55*). Samples were resolved on a 10% Laemmli SDS−polyacrylamide gel as above, Coomassie stained and the receptor bands quantitated using a digital camera (Alpha Innotec).

Protein-Interactions-by-Cysteine-Modification (PICM). PICM analysis was carried out as described previously (*45*). Briefly, a solvent-exposed cysteine was first alkylated with the fluorescein conjugate 5-fluorescein maleimide (5-FM) to a high stoichiometry (>0.9 labels/receptor monomer) by adding 150 μM 5-FM in DMF or DMF alone to receptor containing membranes (5 μM receptor monomer), then incubating for 1 min at 25 °C. The resulting 5-FM labeled and control receptors were subsequently used in in vitro kinase assays as described above.

To control for long-range structural changes upon 5-FM attachment, modified and unmodified receptors were tested in in vitro methylation assays (*45, 58*). Each 5-FM labeled or control receptor in membrane was mixed in buffer (50 mM potassium phosphate, pH 7.0, with NaOH and 0.5 mM EDTA) containing 1 μL of a CheR-containing cytosolic extract (15−20 mg/mL total protein) (*22, 23*). Samples were then allowed to equilibrate for at least 30 min at 25 °C to allow the receptor-CheR complex to form. Methylation was initiated by the addition of a 1:1 mixture of *S*-adenosyl-L-methionine (SAM) and *S*-adenosyl-L-[methyl-^{3}H]methionine ([^{3}H]SAM) to yield a final total SAM concentration of 0.1 mM. The reaction was allowed to proceed for 50, 60, and 70 s then stopped by spotting aliquots on a filter paper and immersing in a 10% w/v trichloroacetic acid (TCA) bath, with subsequent stirring for 10 min. The TCA wash was repeated twice, followed by a pair of 2 min methanol washes to remove residual TCA. Filter papers were placed in eppendorf tubes, 100 μL of 1 M NaOH was added to the filter papers, and each tube was floated in a vial containing scintillation cocktail (Ecoscint H; National Diagnostics). Liberated [^{3}H]methanol partitioned into the scintillation cocktail during an 18 h incubation at 37 °C then was quantitated by scintillation counting.

Standard Deviation. Indicated error ranges represent the standard deviation of the mean for $n \geq 3$.

RESULTS

Production of Cysteine Library. A library of engineered single cysteine-containing receptors spanning the C-terminal half of the signaling domain was created by oligonucleotide-directed mutagenesis. The scanned region encompassed positions Gly388 through Ile419, with the exception of Q390C for which mutagenesis failed. Each of the 31 engineered receptors was overexpressed in strain RP3808,

which lacks the methyltransferase and methylesterase adaptation enzymes (*51*). The resulting receptor population was homogeneous with respect to methylation, having glutamines at positions 295 and 309 and glutamates at 302 and 491. In all cases, the cysteine-containing receptors accumulated to essentially the same level as overexpressed wild-type receptor and were isolated in native *E. coli* membranes. As previously observed in other cysteine-scanning studies of the aspartate receptor, despite the presence of two symmetric mutant cysteines in each receptor homodimer, SDS−PAGE revealed that the level of disulfide-linked dimer after membrane isolation and storage was generally less than 10% of the total receptor population.

Chemical Reactivity and Solvent Exposure of Engineered Cysteines. To map out secondary structural elements, patterns of solvent exposure and burial were analyzed using a chemical reactivity assay. This assay assesses the ability of a given cysteine to react with 5-iodoacetamido fluorescein (5-IAF), a fluorescent, thiol-specific alkylating agent. The large size of this aqueous probe and its multivalent negative charge prevent it from entering the cores of folded proteins. Previous studies of a known structure have demonstrated a strong correlation between the 5-IAF reactivity of a position and its solvent exposure (*43*). Additional control studies using a neutral aqueous probe yielded the same correlation, indicating that steric accessibility, rather than local electrostatics, is the primary determinant of chemical reactivity (*45*).

In the present study, the reactivity assay began by incubating *E. coli* membrane containing a given cysteine-containing receptor with the probe at 25 °C for 5 min, at which time the reaction was split. Half of the sample was quenched with excess β-mercaptoethanol, while the other half was denatured with SDS and heat (95 °C) before quenching. The latter step was designed to ensure that the 5-IAF-labeling reaction would continue after receptor unfolding, thereby providing the maximal extent of labeling attainable for a solvent-exposed cysteine under the indicated reaction conditions. Reaction with the unfolded receptor served as a positive control and yielded the maximal labeling for each engineered receptor. The resulting samples were resolved on SDS−PAGE gels and the fluorescence of the labeled receptor bands was quantitated via digital imaging. Following fluorescence quantitation, gels were stained with Coomassie and the receptor bands were digitized and integrated, enabling correction of the raw fluorescence for variations in receptor amounts. The chemical reactivity ratio is defined as the ratio of fluorescent labeling in the native state relative to that in the denatured state. This ratio can vary from zero for a buried cysteine that is totally inaccessible to the probe in the folded state, up to unity for an exposed cysteine that is equally accessible in the native and denatured states. In practice, experimental conditions were chosen such that the most exposed positions yielded ratios less than 0.8, thereby avoiding saturation of these positions with label.

A subset of 10 engineered receptors, G388C, E389C, G391C, R402C, N403C, S406C, A409, Q410C, K413C, and E414C were found to be highly reactive, yielding reactivity ratios above 0.4, as illustrated in Figure 2. It follows that these positions are solvent exposed. Another subset of eight positions was found to be highly protected from labeling in the folded state, yielding reactivities below 0.2. These

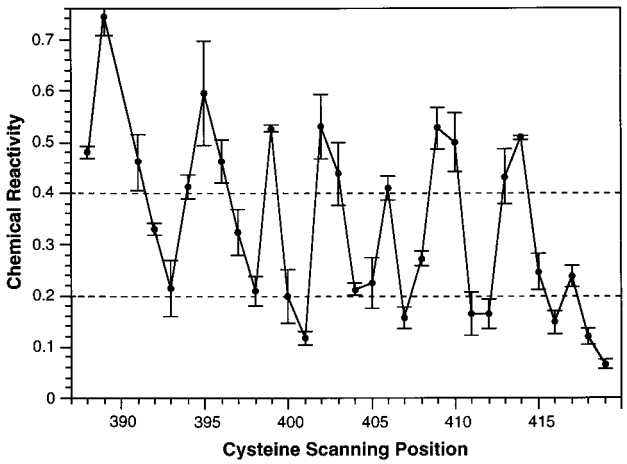

FIGURE 2: Chemical reactivities of residues G388C through I419C in the signaling domain. The chemical reactivity of each cysteine-containing receptor in isolated *E. coli* membranes was measured by incubating the sulfhydryl-specific probe 5-IAF for 5 min at 25 °C. Two aliquots were then removed from the reaction and one quenched with excess β-mercaptoethanol. The other aliquot was denatured with heat and SDS and allowed to react with the probe for an additional 3 min before quenching. The ratio of receptor labeling in the native sample to the denatured sample is defined as the chemical reactivity, with corrections made for variations in the amount of receptor. Positions with a reactivity of below 0.2, indicated by the lower dashed line, are classified as highly buried. Positions exhibiting a reactivity above 0.4, indicated by the upper dashed line, are classified as solvent exposed.

positions, V401C, R407C, A411C, A412C, I415C, K416C, L418C, and I419C are classified as buried. The remaining positions yielded intermediate reactivities and no attempt was made to classify their solvent exposures. When the highly exposed and buried residues were modeled on various secondary structures, it was found that the best segregation of exposure and burial was provided by a 3.5 residue/turn α-helix termed α8, ranging approximately from V401 to I419 or beyond (see Discussion). This is the periodicity expected for a helix in a coiled-coil or four helix bundle. Interestingly, positions G388C through G391C, which lie just N-terminal to the newly detected helix α8, yield the highest peak of chemical reactivity in the scanned region. A variety of evidence suggests that this highly exposed region forms a hairpin turn between the adjacent α7 and α8 helices (see Discussion).

Identification of Residues Critical for Receptor Function in Vivo. The effect of each cysteine substitution on receptor function in vivo was determined by the chemotaxis swarm assay (*52*). In this assay, a strain that lacks the aspartate receptor is transformed with an engineered receptor to test its ability to restore chemotaxis up aspartate gradients. The assay detects only the most serious receptor defects, since receptor overexpression and the adaptation branch of the pathway can correct for subtle defects (*22*, *23*). Each engineered receptor was expressed in strain RP8611, which lacks the aspartate receptor, but retains the adaptation enzymes CheR and CheB (*51*). When the resulting cells were spotted on minimal media plates containing aspartate, the cells generated an outward-moving halo as they metabolized the attractant and migrated up the resulting gradient. The rate of halo expansion is termed the swarm rate. By subtracting the swarm rates measured on plates containing and lacking aspartate, the aspartate-specific swarm rate could

be calculated as a quantitative measure of receptor function in vivo.

The aspartate-specific swarm rate, shown in Figure 3A, ranged from zero to a rate 2.5-fold higher than that observed for cells expressing the wild-type receptor. All the engineered receptors were overexpressed at levels comparable to the overexpressed wild-type receptor; thus, those that failed to restore swarming lacked function in vivo, while those that did restore swarming were functional, or even superactive in certain cases. Cysteine substitutions were defined as inhibitory if they diminished the aspartate-specific swarm ratio by 2-fold or more. Altogether, 19 of the thirty-one cysteine substitutions were found to inhibit receptor function in vivo: G388C, G391C, R392C, F394C, A395C, V397C, A398C, E400C, V401C, R402C, L404C, S406C, S408C, A409C, A412C, K413C, I415C, L418C, and I419C. Interestingly, the locations of these inhibitory substitutions fall on both faces of the helix identified by solvent exposure patterns (see Discussion), indicating that both faces are functionally important. In the region just N-terminal to the helix, the Gly residues at positions 388 and 391 are both essential for receptor activity, consistent with the proposal that they are critical for the conformation of an interhelical hairpin turn.

Identification of Residues Critical for Receptor-Mediated Kinase Regulation in Vitro. The effect of each cysteine substitution on receptor function was also measured in an in vitro assay that directly monitors receptor-mediated kinase regulation (*14, 15*). Receptors in isolated *E. coli* membranes were combined with soluble chemotaxis components to reconstitute the receptor-kinase signaling complex, composed of at least two molecules of receptor, two molecules of the coupling protein CheW, and two molecules of the histidine kinase CheA (*13, 59*). Excess CheY was also present to serve as the phosphoacceptor, and the formation of phospho-CheY was quantitated to follow the reaction time course. The assay conditions ensured that virtually all of the kinase CheA was bound to receptor and that the rate-limiting step in the phosphorylation cascade is the autophosphorylation of CheA. The wild-type receptor maintains the kinase in a highly active state in the absence of aspartate; however, the addition of aspartate to the receptor downregulates kinase activity at least 100-fold, to levels which are undetectable (*14, 15, 45*). Each receptor-kinase complex containing a given mutant receptor was assayed for its ability to activate CheA, and to downregulate CheA upon addition of saturating aspartate.

A subset of 13 of the 31 reduced cysteine-containing receptors, shown in Figure 3B, failed to generate significant kinase activation: G388C, E389C, G391C, R392C, G393C, A395C, A398C, E400C, V401C, R402C, S406C, S408C, and L418C. Like the cysteine substitutions found to be inhibitory in vivo, these fall on both faces of the helix, further supporting the notion that both faces of this helix are involved in critical contacts necessary for receptor function. Another subset of seven engineered receptors were found that were able to activate the kinase to appreciable levels, but were unable to downregulate the kinase in the presence of saturating aspartate concentrations: F394C, V397C, L404C, A411C, A412C, I415C, and I419C. These seven cysteines are defined as lock-on substitutions, because they trap the receptor in the kinase activating state, even in the presence of sufficient aspartate to saturate ligand binding. The possibility that the lock-on cysteine substitutions prevented ligand binding was excluded by in vitro methylation assays (not shown), where each of the locked-on receptors yielded an aspartate-induced increase in the methylation rate at the

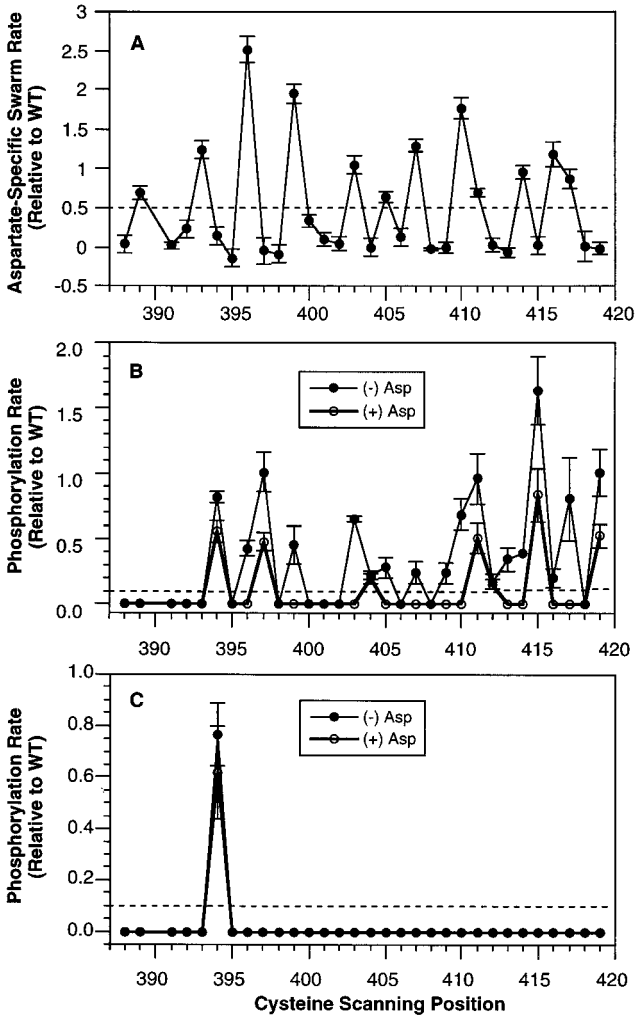

FIGURE 3: In vivo and in vitro activity of the engineered cysteine-containing receptors. (A) To carry out the in vivo chemotactic swarm assay, each engineered receptor was expressed in an *E. coli* strain lacking the aspartate receptor and the ability of each receptor to restore chemotaxis up an aspartate gradient was quantitated. The aspartate-specific swarm rate represents the difference between the chemotactic swarm rates measured on minimal media plates containing and lacking aspartate, respectively, with subsequent normalization to the wild-type receptor. Receptors yielding rates below the dashed line (50% of wild-type) are classified as inhibitory. (B) To carry out the in vitro receptor-regulated kinase assay, each engineered receptor in isolated *E. coli* membranes was reconstituted with purified CheA, CheW, and CheY. CheA autophosphorylation and subsequent phospho-transfer to CheY was initiated by the addition of [^{32}P]ATP and allowed to proceed for a fixed time before quenching. The level of product [^{32}P]phospho-CheY was then quantitated and used to determine the rate of the slow step in the reaction sequence, namely the autophosphorylation of CheA. To facilitate comparison, all rates were normalized to the rate observed for the wild-type receptor-kinase ternary complex in the absence of aspartate. The fine and bold lines, respectively, connect data points obtained for the reduced receptor in the absence and presence of 1 mM aspartate. Cysteine substitutions which reduce kinase activation by the reduced apo receptor to a level below 10% of the wild-type rate, as indicated by the lower dashed line, are classified as inhibitory. Filled triangles denote lock-on cysteine positions where the cysteine substitution prevents full aspartate-induced kinase downregulation. (C) Same as panel B, except that each engineered receptor was oxidized to form an intersubunit disulfide bond prior to initiating the receptor-regulated kinase assay.

same ligand concentration (1 mM aspartate) used in the phosphorylation assay (*45, 58*). Significantly, while the cysteine substitutions that blocked kinase activation were distributed on both surfaces of helix α8, the lock-on cysteines were found only on its buried face (see Discussion). It follows that the buried helix face is especially critical for receptor downregulation. Interestingly, the highest density of deleterious cysteine substitutions occurs at positions 388−395, the region which contains the proposed α7-α8 interhelical hairpin turn and is one of the most highly conserved regions of the methyl-accepting taxis receptor superfamily (*10, 60*).

Altogether, 11 of the 13 cysteine substitutions that constitutively inhibited receptor-mediated kinase activation in vitro were also found to be inhibitory in vivo. These 11 substitutions slow the rate of CheA autophosphorylation, thereby slowing phospho-transfer and the formation of phospho-CheY, which is needed to regulate the switch elements of the flagellar motor (*61*). At the other extreme, six of the seven lock-on cysteine substitutions that constitutively activated the kinase in vitro were found to block receptor function in vivo, as expected. The exceptions to these generalities included the E389C, G393C and A411C substitutions, which prevented kinase activation or downregulation in vitro but were active in vivo, suggesting compensation by the adaptation system present in the cellular setting. Interestingly, two of the nineteen substitutions that blocked receptor function in vivo were partially active in vitro, specifically A409C and K413C, suggesting that these substitutions may inhibit a receptor function other than CheA regulation, such as receptor adaptation. Usually, however, damaged receptors were nonfunctional both in vivo and in vitro.

Probing Intersubunit Contacts by Disulfide Scanning. Each single cysteine substitution introduces a pair of symmetric cysteines into the receptor homodimer, enabling disulfide formation under oxidizing conditions using Cu(II)(1,10-phenanthroline)$_3$ to initiate the reaction (*55, 56*). By oxidizing successive cysteine substitutions, a disulfide bond can be effectively walked through the receptor. Strong oxidizing conditions are used to drive disulfide formation toward completion, followed by analysis of these cross-linked receptor in the in vitro kinase assay (*45*). Wild-type receptor, containing no cysteines, is unable to cross-link and is largely unaffected by the oxidant treatment. Under strong oxidizing conditions, all the scanned cysteine positions yielded efficient intersubunit disulfide formation exceeding 60% completion, which reflects the extensive conformational dynamics of the cytoplasmic domain (*62*). Most of these disulfide bonds trap thermal collisions away from the active conformation. Only the 394−394′ disulfide, which formed to a level exceeding 80%, also retained significant receptor-mediated kinase activation in vitro as illustrated in Figure 3C**.** The F394C substitution itself was found to lock the receptor in the kinase-activating state (see above), and this lock-on character is retained when the 394−394′ disulfide is formed. This indicates that the locked-on receptor structure induced by the cysteine substitution 394−394′ is preserved in the disulfide cross-linked form of the receptor, and that the two cysteines are proximal to one another in the receptor state that activates the kinase.

To ascertain whether the 394−394′ disulfide cross-links two subunits within the dimer or rather forms during collisions between dimers, a double-cysteine-containing receptor was engineered containing F394C and N36C, since the latter cysteine is known to form an intradimer cross-link (*30*). Upon oxidation, the double-cysteine-containing receptor N36C/F394C initially forms three species of disulfide cross-linked receptors, as visualized on SDS−PAGE. However, by the end of the standard 20 min oxidation, the two dimers representing the 36−36′ and 394−394′ single disulfide species are fully converted to the third species with intermediate mobility which represents the 36−36′/394−394′ double-disulfide dimer. It follows that the 394−394′ disulfide forms between the two subunits in the homodimer. Since the 394 position lies within the proposed loop between the α7 and α8 helices (see Discussion), it follows that the loop must lie near the subunit interface of the dimer, at least in the kinase-activating state.

Probing Intrasubunit Contacts by Inroducing Targetted Cysteine Pairs. To determine whether helices α7 and α8 form a helical hairpin, a set of double-cysteine mutants was created. Each mutant possessed one cysteine substituted at the buried A411C position on α8, together with a second cysteine at one of six selected **a** or **d** positions on the buried face of α7 (I363C, I366C, A370C, T373C, A377C, and A380C). If helices α7 and α8 are adjacent to one another as in a hairpin configuration, then it should be possible to generate interhelix disulfide bonds across the buried helix−helix interface using mild oxidation conditions to provide more selective disulfide formation than the strong oxidizing conditions utilized above (*44, 57*). The results reveal that a mild, 1 min oxidation reaction generates detectable intrasubunit disulfide formation for only two cysteine pairs: A411C−A370C (30% completion) and A411C−T373C (20% completion). In both cases, the intrasubunit disulfide was detected by the mobility increase it generated on SDS−PAGE, which was reversed by reducing agent (see ref *63*). It follows, therefore, that helices α7 and α8 are adjacent in space such that the A411C/A370C and A411C/T373C cysteine pairs are in sufficient proximity to collide and form a disulfide bond, while the other cysteine pairs are more distal. The simplest model is one in which helices α7 and α8 are separated by a tight turn that enables them to form an antiparallel helical hairpin, as well as the engineered interhelix disulfide bonds A411C−A370C and A411C−T373C.

Protein Interactions by Cysteine Modification (PICM). A critical docking or regulatory surface can be mapped out by modifying surface-exposed cysteines with a bulky probe, then testing the effects of the modification on receptor activity (*45*). Positions where probe attachment blocks receptor-mediated kinase activation without significantly perturbing receptor structure are likely to lie within the docking face for the kinase CheA or the coupling protein CheW. Surface cysteines V396C, G399C, N403C, A409C, Q410C, K413C, and E414C were chosen since all were solvent accessible, all retained measurable kinase activation in the in vitro assay, and all were labeled to a stoichiometry exceeding 90% with the probe 5-fluorescein maleimide (5-FM). Four of the seven positions, N403C, Q410C, K413C, and E414C, could be modified with the probe and still retain at least 50% of the unmodified kinase activation observed in the unmodified

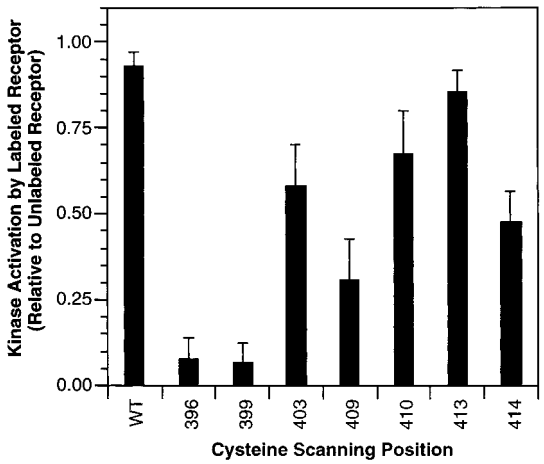

FIGURE 4: The protein interaction-by-cysteine-modification (PICM) assay. Solvent exposed positions in the scanned region were stoichiometrically labeled with 5-FM to observe the effect of this bulky probe on receptor-mediated kinase activation in vitro. Each engineered cysteine shown was reacted with probe or, as a control, incubated with the solvent for the probe, DMF. The resulting modified and control receptors were used in the receptor-coupled kinase assay (see legend, Figure 3B). The resulting rates of phospho-CheY formation observed in the absence of aspartate are given as a ratio of the rate observed for the modified receptors to the rate for the same unmodified, control receptor.

state, as well as full kinase downregulation by aspartate binding as seen in Figure 4. By contrast, modification of the A409C residue yielded 70% inhibition, while modification of V396C or G399C yielded at least 90% inhibition relative to the unmodified receptor.

These modification-induced losses of kinase activation could, in principle, arise from large changes in the structure of the cytoplasmic domain. The in vitro methylation assay was used to test this possibility (*45*, *58*). The rate of CheR-catalyzed methylation of the adaptation glutamates is highly sensitive to perturbations of cytoplasmic domain structure (*22*, *64*). Engineered receptors were assayed for their ability to be methylated in the modified and unmodified states. In all cases, the 5-FM modified receptors were methylated at levels comparable both to the unmodified receptor and to the wild-type receptor, and each modified receptor also showed the characteristic 2-fold increase in methylation upon the addition of aspartate (*45*, *58*). It follows that the inhibitory effects of the 5-FM probe are due to localized perturbation of a kinase docking or regulatory surface rather than to long-range perturbations of cytoplasmic domain structure.

DISCUSSION

The present cysteine- and disulfide-scanning study generates a low-resolution structural map of the signaling domain by analyzing the solvent exposure of individual positions and by identifying pairs of positions that lie in close proximity. The chemical reactivity of a cysteine residue scanned from position G388C through I419C reveals a periodic pattern of highly reactive, exposed positions and unreactive buried positions beginning at approximately V401C and continuing through the last residue scanned, I419C. Mapping these highly exposed and buried positions on various secondary structure models reveals that an α-helix with 3.5 residues/turn provides the best segregation of exposed and buried positions on opposite structural faces. This helix, termed α8, is illustrated in Figure 5A. The detected periodicity of 3.5 residues/turn is indicative of a helix involved in a coiled-coil or four helix bundle interaction. Further evidence supporting this secondary structure assignment is provided by a sequence alignment for the cytoplasmic domains of over 60 homologous taxis receptors, which reveals a highly conserved heptad pattern in the α8

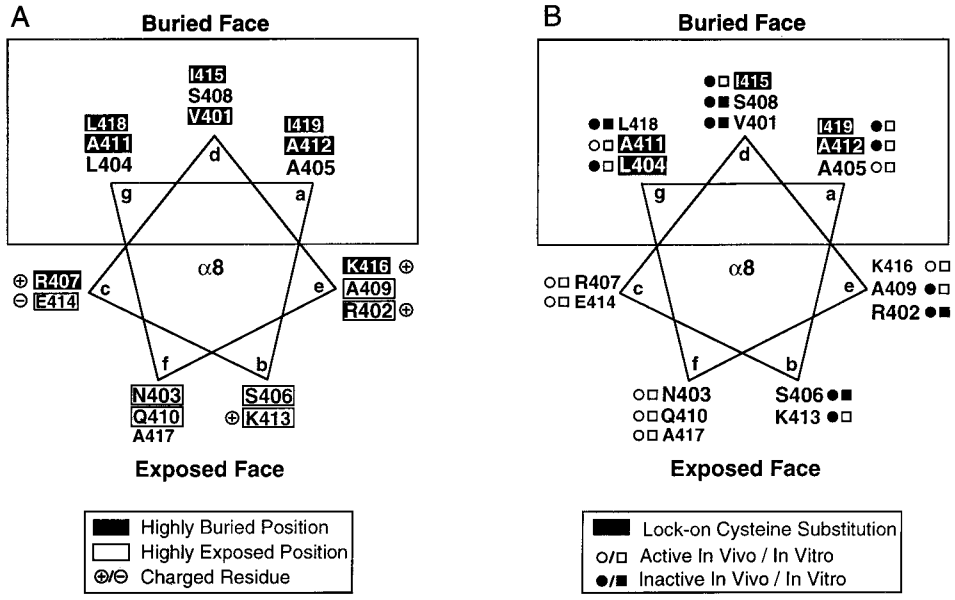

FIGURE 5: Helical wheel model for positions G393 through I419 of the signaling domain illustrating the chemical reactivities and activity effects of each cysteine substitution. (A) Chemical reactivity data. White rectangles denote solvent-exposed positions with high chemical reactivities, while black rectangles indicate buried positions yielding low chemical reactivities (see Figure 2). The buried face of the helix is designated by the large open box and charged residues are noted. **B)** In vivo and in vitro activity data. Black rectangles highlight lock-on cysteine substitutions that prevent full aspartate-induced kinase downregulation in the in vitro kinase assay (see Figure 3B). Small open and closed circles indicate cysteine substitutions found to retain activity or inhibit function in vivo, respectively (see Figure 3A). Small open and closed squares denote substitutions which retain activity or inhibit function in the in vitro kinase assay, respectively (see Figure 3B).

region wherein the **a**, **d**, and **g** positions of the heptad are generally nonpolar while the remaining **b**, **c**, **e**, and **f** are often polar or charged (*10, 11*). Thus, helix α8 appears to be a conserved, strongly amphiphilic element within the signaling domain.

A previous study defined another amphiphilic helix, α7, spanning at least from S355 to R386. The present cysteine scan reveals that positions G388C, E389C, and G391C, located in the proposed linker between helical regions α7 and α8, are highly exposed and yield the highest peak chemical reactivity. Moreover, cysteine substitution at the G388 and G391 positions fully destroy receptor function in both the in vivo chemotactic swarm assay and the in vitro receptor-regulated kinase assay, consistent with a model in which these glycines allow a hairpin turn between the α7 and α8 helices. Such a turn would explain the rapid interhelix disulfide bond formation observed between specific pairs of cysteines located on the buried faces of α7 and α8 (A411C−A370C and A411C−T373C). Together these data indicate that the α7 and α8 helices form an intrasubunit helical hairpin. This hairpin is conserved, as indicated by the strong conservation of both helices and the two glycines in sequence alignment. Moreover, an analysis of insertions or deletions (indels) of the aligned receptor superfamily sequences revealed that indels in helix α7 are matched by indels of similar length in α8 (*10, 11*), providing additional support for the conserved hairpin structure.

The buried surface area detected on helices α7 and α8 is larger than expected, however, for helices involved in a simple coiled-coil helical hairpin wherein only the a and d spokes of the heptad repeat are highly buried (*45, 60*). Instead, the present model proposes that the two symmetric α7/α8 hairpins of the dimer associate to form a four helix bundle. Evidence supporting this picture is provided by the intersubunit disulfide bonds A387C−A387C′ (*45*) and F394C−F394C′ which retain kinase regulation or constitutively activate the kinase, respectively. These intradimer disulfides both lie within the proposed hairpin turn between helices α7 and α8, indicating that the turn lies at or near the subunit interface in the functional conformations of the receptor. Both disulfides have been shown to form between subunits in the same dimer by pairing them with the N36C−N36C′ intradimer disulfide (*30, 56, 63*). Together, these results suggest a working model in which helices α7 and α8, along with their symmetric counterparts α7′ and α8′ from the other subunit, pack together in a four helix bundle that accounts for the large buried faces on the component helices.

Only three buried positions within the scanned region of the proposed helical bundle exhibit highly conserved polar side chains. Specifically, S356 located on an a spoke of helix α7 is found to be serine or threonine in 64% of the aligned sequences, while T373 at a d position is threonine or serine in 100% of the sequences, and S408 on a d spoke of helix α8 is serine or threonine in 89% of the family members. Studies of other helix−helix interactions have shown that buried polar residues can stabilize a specific register or orientation of packed helices, suggesting that these conserved polar side chains help define the architecture of the four helix bundle (*65, 66*). The exposed face of helix α7 has been shown to be composed of both polar and nonpolar residues, where the latter are proposed to assist CheA and/or CheW docking (*45*). The exposed face of the scanned region of

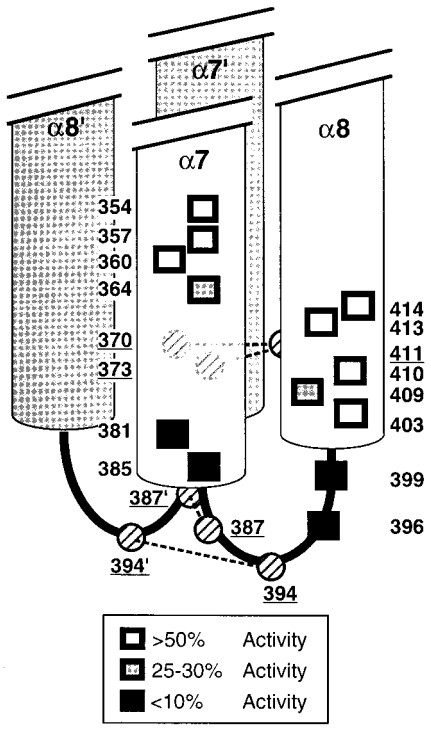

FIGURE 6: Model of the signaling domain composed of helices α7 and α8, indicating the results of the disulfide scanning and PICM study (*45*). Cylinders represent experimentally defined helical regions, where the helix ends are not precisely determined (*43, 45*). Underlined cysteine positions connected by dashed lines were found to form disulfides rapidly under mild oxidizing conditions (A411C−A370C, A411C−T373C), or to retain kinase activation in the in vitro receptor-regulated kinase assay (A387C−A387C′, F394C−F394C′). For the PICM study, open squares indicate cysteine positions at which 5-FM attachment maintains at least 50% of the kinase activation observed for the unlabeled receptor. The gray and black squares denote surface positions at which 5-FM labeling inhibits kinase activation 70% or at least 90%, respectively.

helix α8, by contrast, is composed of exclusively polar and charged residues with only two exceptions: A409 and A417. The five charged residues, R402, R407, K413, E414, and K416 all fall on this exposed face of the helix, or at the interface between the exposed and buried regions where a long side chain could enable the terminal charge to reach the solvent.

Many cysteine substitutions in the region scanned yielded diminished receptor activity both in vivo and in vitro as previously observed in a cysteine scan of the N-terminal helix in the signaling domain (*45*). In helix α8, 58% of the cysteine substitutions were inhibitory in vivo and 26% inhibited receptor-mediated kinase regulation in vitro, as illustrated in Figure 5B. Buried positions on helix α8 were especially sensitive to perturbation as indicated by their high percentage of inhibitory positions, 78% in vivo and 33% in vitro. The exposed face was also susceptible, although to a lesser degree where 40% of cysteine substitutions at exposed positions were found to be inhibitory in vivo and 26% were inhibitory in vitro. The sensitivity of receptor function to helix α8 surface substitutions is in sharp contrast to the helix α5/α6 region where surface cysteine substitutions inhibited receptor function in vivo and in vitro at a frequency of only 6% and 11%, respectively (*43, 44*). Instead, the results for α8 were more similar to those obtained for helix α7 of the signaling

domain, where surface cysteine substitutions diminished receptor function in vivo and in vitro at a frequency of 58 and 50%, respectively (*45*). Together, these results suggest that the buried face of helices α7 and α8 are critical for receptor function and that the exposed faces are important as well.

The buried face of helix α8 is especially critical for kinase downregulation as indicated by fact that all five lock-on cysteine substitutions localize to this face. Similarly, all of the lock-on cysteines observed in helix α7 are located on its buried face (*45*). Given that these helices associate in a four helix bundle, the buried core of the bundle is proposed to control kinase downregulation.

The recently developed PICM method has been used previously to map out positions on helix α7 that interact with the kinase CheA and/or the coupling protein CheW (*45*). Here the method implicated three positions in CheA/CheW docking or regulation since attachment of a bulky probe at these surface cysteine locations significantly inhibits kinase activation (S396C, A399C and A409C) as seen in the model presented in Figure 6. The diminished activity of these modified receptors is due to localized effects since probe attachment did not perturb the methylation rates of the adaptive glutamates in the in vitro CheR methyltransferase assay. Interestingly, the two positions at which probe attachment most strongly inhibited kinase activation, S396C and A399C, lie in or near the α7-α8 loop while the third position, A409C, lies nearby on the N-terminal region of helix α8. Together, these results suggest that the kinase interaction surface comprises the C-terminal end of helix α7, the loop between helices α7 and α8, and perhaps the N-terminus of the α8 helix. The detection of this well-defined surface supports the hypothesis that the signaling domain is an independent folding unit responsible for binding CheA and CheW (*49*), thereby playing a central role in kinase regulation. More generally, the conserved nature of helices α7 and α8, as well as the hairpin turn between them, indicates that the signaling domain exhibits a similar fold and function in all members of the taxis receptor superfamily.

ACKNOWLEDGMENT

The authors gratefully acknowledge Drs. Jerry Hazelbauer, Ikuro Kawagishi, Sandy Parkinson, and Jeff Stock for stimulating discussions.

REFERENCES

1. Mowbray, S. L., and Sandgren, M. O. J. (1998) *J. Struct. Biol. 124*, 257−275.
2. Djordjevic, S., and Stock, A. M. (1998) *J. Struct. Biol. 124*, 189−200.
3. Falke, J. J., Bass, R. B., Butler, S. L., Chervitz, S. A., and Danielson, M. A. (1997) *Annu. Rev. Cell Dev. Biol. 13*, 457−512.
4. Wurgler-Murphy, S. M., and Saito, H. (1997) *Trends Biochem. Sci. 22*, 172−176.
5. Hoff, W. D., Jung, K. H., and Spudich, J. L. (1997) *Annu. Rev. Biophys. Biomol. Struct. 26*, 223−258.
6. Stock, J. B., and Surette, M. G. (1996) in *Escherichia coli and Salmonella Cellular and Molecular Biology* (Neidhardt, F. C., Ed.) pp 1103−1129, ASM Press, Washington DC.
7. Blair, D. F. (1995) *Annu. Rev. Microbiol. 49*, 489−522.
8. Swanson, R. V., and Simon, M. I. (1994) *Curr. Biol, 4*, 234−237.
9. Parkinson, J. S. (1993) *Cell 73*, 857−871.
10. Le Moual, H., and Koshland, D. E., Jr. (1996) *J. Mol. Biol. 261*, 568−585.
11. Danielson, M. A. (1997) *The molecular mechanism of transmembrane signaling and kinase regulation by the aspartate receptor of bacterial chemotaxis*, Ph.D. Thesis, Department of Chemistry and Biochemistry, University of Colorado, Boulder, CO.
12. Krikos, A., Mutoh, N., Boyd, A., and Simon, M. I. (1983) *Cell 33*, 615−622.
13. Gegner, J. A., Graham, D. R., Roth, A. F., and Dahlquist, F. W. (1992) *Cell 70*, 975−982.
14. Borkovich, K. A., Kaplan, N., Hess, J. F., and Simon, M. I. (1989) *Proc. Natl. Acad. Sci. U.S.A. 86*, 1208−1212.
15. Ninfa, E. G., Stock, A. M., Mowbray, S. L., and Stock, J. B. (1991) *J. Biol. Chem. 266*, 9764−9770.
16. Schuster, S. C., Swanson, R. V., Alex, L. A., Bourret, R. B., and Simon, M. I. (1993) *Nature 365*, 343−347.
17. Baumgartner, J. W., Kim, C., Brissette, R. E., Inouye, M., Park, C., and Hazelbauer, G. L. (1994) *J. Bacteriol. 176*, 1157−1163.
18. Krikos, A., Conley, M. P., Boyd, A., Berg, H. C., and Simon, M. I. (1985) *Proc. Natl. Acad. Sci. U.S.A. 82*, 1326−1330.
19. Utsumi, R., Brissette, R. E., Rampersaud, A., Forst, S. A., Oosawa, K., and Inouye, M. (1989) *Science 245*, 1246−1249.
20. Tatsuno, I., Lee, L., Kawagishi, I., Homma, M., and Imae, Y. (1994) *Mol. Microbiol. 14*, 755−762.
21. Moe, G. R, Bollag, E., and Koshland, D. E., Jr. (1989) *Proc. Natl. Acad. Sci. U.S.A. 86*, 5683−5687.
22. Chervitz, S. A., Lin, C. M., and Falke, J. J. (1995) *Biochemistry 34*, 9722−9733.
23. Chervitz, S. A., and Falke, J. J. (1995) *J. Biol. Chem. 270*, 24043−24053.
24. Pakula, A. A., and Simon, M. I. (1992) *Proc. Natl. Acad. Sci. U.S.A. 89*, 4144−4148.
25. Wang, J. X., Balazs, Y. S., and Thompson, L. K. (1997) *Biochemistry 36*, 1699−1703.
26. Jeffrey, C. J., and Koshland, D. E. (1993) *Protein Sci. 2*, 559−566.
27. Hughson, A. G., Lee, G. F., and Hazelbauer, G. L. (1997) *Protein Sci. 6*, 315−322.
28. Lee, G. F., Burrows, G. G., Lebert, M. R., Dutton, D. P., and Hazelbauer, G. L. (1994) *J. Biol. Chem. 269*, 29920−29927.
29. Baumgartner, J. W., and Hazelbauer, G. L. (1996) *J. Bacteriol. 178*, 4651−4660.
30. Milburn, M. V., Prive, G. G., Milligan, D. L., Scott, W. G., Yeh, J., Jancarik, J., Koshland, D. E., Jr., and Kim, S. H. (1991) *Science 254*, 1342−1347.
31. Chervitz, S. A., and Falke, J. J. (1996) *Proc. Natl. Acad. Sci. U.S.A. 93*, 2545−2550.
32. Hughson, A. G., and Hazelbauer, G. L. (1996) *Proc. Natl. Acad. Sci. U.S.A. 93*, 11546−11551.
33. Ottemann, K. M., Thorgeirsson, T. E., Kolodziej, A. F., Shin, Y. K., and Koshland, D. E., Jr. (1998) *Biochemistry 37*, 7062−7069.
34. Zhang, Y. H., Gardina, P. J., Kuebler, A. S., Kang, H. S., Christopher, J. A., and Manson, M. D. (1999) *Proc. Natl. Acad. Sci. U.S.A. 96*, 939−944.
35. van Iwaarden, P., Pastore, J. C., Konings, W. N., and Kaback, H. R. (1991) *Biochemistry 30*, 9595−9600.
36. Sahin-Toth, M., and Kaback, H. R. (1993) *Protein Sci. 2*, 1024−1033.
37. Frillingos, S., Sun, J., Gonzalez, A., and Kaback, H. R. (1997) *Biochemistry 36*, 269−273.
38. Yu, H. B., Kono, M., McKee, T. D., and Oprian, D. D. (1995) *Biochemistry 34*, 14963−14969.
39. Kono, M., Yu, H. B., and Oprian, D. D. (1998) *Biochemistry 37*, 1302−1305.
40. Akabas, M. H., Kaufmann, C., Archdeacon, P., and Karlin, A. (1994) *Neuron 13*, 919−927.
41. Akabas, M. H., Stauffer, D. A., Xu, M., and Karlin, A. (1992) *Science 258*, 307−310.
42. Falke, J. J., Sternberg, D. W., and Koshland, D. E., Jr. (1986) *Biophys. J. 49*, 20−25.

43. Danielson, M. A., Bass, R. B., and Falke, J. J. (1997) *J. Biol. Chem. 272*, 32878−32888.
44. Butler, S. L., and Falke, J. J. (1998) *Biochemistry 37*, 10746−10756.
45. Bass, R. B., and Falke, J. J. (1998) *J. Biol. Chem. 273*, 25006−25014.
46. Trammell, M. A., and Falke, J. J. (1999) *Biochemistry 38*, 329−336.
47. Nara, T., Kawagishi, I., Nishiyama, S., Homma, M., and Imae, Y. (1996) *J. Biol. Chem. 271*, 17932−17936.
48. Nishiyama, S., Nara, T., Homma, M., Imae, Y., and Kawagishi, I. (1997) *J. Bacteriol. 179*, 6573−6580.
49. Ames, P., Yu, Y. A., and Parkinson, J. S. (1996) *Mol. Microbiol. 19*, 737−746.
50. Surette, M. G., and Stock, J. B. (1996) *J. Biol. Chem. 271*, 17966−17973.
51. Liu, J. D., and Parkinson, J. S. (1989) *Proc. Natl. Acad. Sci. U.S.A. 86*, 8703−8707.
52. Adler, J. (1966) *Science 153*, 708−716.
53. Bibikov, S. I., Biran, R., Rudd, K. E., and Parkinson, J. S. (1997) *J. Bacteriol. 179*, 4075−4079.
54. Laemmli, U.K. (1970) *Nature 227*, 680−685.
55. Careaga, C. L., and Falke, J. J. (1992) *J. Mol. Biol. 226*, 1219−1235.
56. Falke, J. J., and Koshland, D. E., Jr. (1987) *Science 237*, 1596−1600.
57. Chen, X., and Koshland, D. E., Jr. (1997) *Biochemistry 36*, 11858−11864.
58. Chelsky, D., Gutterson, N. I., and Koshland, D. E., Jr. (1984) *Anal. Biochem. 141*, 143−148.
59. Levit, M. N., Liu, Y., and Stock, J. B. (1998) *Mol. Microbiol. 30*, 459−466.
60. Marshall, C. J. (1995) *Cell 80*, 179−185.
61. Macnab, R. M. (1987) in *Escherichia coli and Salmonella: Cellular and Molecular Biology* (Neidhardt, F. C., Ed.) pp 70−83, ASM Press, Washington DC.
62. Seeley, S. K., Weis, R. M., and Thompson, L. K. (1996) *Biochemistry 35*, 5199−5206.
63. Falke, J. J., Dernburg, A. F., Sternburg, D. A., Zalkin, N., Milligan, D. L., and Koshland, D. E., Jr. (1988) *J. Biol. Chem. 263*, 14850−14858.
64. Bogonez, E., and Koshland, D. E., Jr. (1985) *Proc. Natl. Acad. Sci. U.S.A. 82*, 4891−4895.
65. Lumb, K. J., and Kim, P. S. (1998) *Biochemistry 37*, 13042.
66. Oakley, M. G., and Kim, P. S. (1998) *Biochemistry 37*, 12603−12610.

BI9908179